

CHAOTIC DYNAMICS OF COHERENT STRUCTURES

L. SIROVICH

Center for Fluid Mechanics and the Division of Applied Mathematics, Brown University, Providence, RI 02912, USA

A variety of chaotic flows evolving in relatively high-dimensional spaces are considered. It is shown through the use of an optimal choice of basis functions, which are a consequence of the Karhunen-Loeve procedure, that an accurate description can be given in a relatively low-dimensional space. Particular examples of this procedure, which are presented, are the Ginzburg-Landau equation, turbulent convection in an unbounded domain and turbulent convection in a bounded domain.

1. Introduction

The overall view of turbulence has undergone considerable change over the past decade or two. This new perspective results in part from what might be called *chaotic dynamics*, a body of ideas based on the papers of Lorenz [1], Ruelle and Takens [2] and Feigenbaum [3], with much of this material now in monographs [4-6; see also 7]. The other new ingredient is the notion of *coherent structures*. This idea goes back more than thirty years to the observations of Theodorsen [8] and Townsend [9] who pointed out the existence of large-scale organized motions in turbulent shear flows. On the experimental side the visualizations of Kline et al. [10], Brown and Roshko [11] and Falco [12] lend support to the presence of such organized structures in a variety of flow situations. Conditional sampling techniques and other criteria have been advanced by Blackwelder and Kaplan [13], Lu and Willmarth [14] and Hussain [15] for the detection of coherent structures; see Cantwell [16] for a survey. But with one exception (see below) the circumstances under which a coherent structure is thought to be present remain subjective, poorly defined, and certainly lack the crispness required of a scientific definition. Questioning after coherent structures is reminiscent of the search for the holy grail in Arthurian times [17].

An important consequence of this body of ideas is the departure from the traditional statisti-

cal approach of Taylor [18] and von Karman [19]. Turbulence is now more universally regarded not as *probabilistic randomness* but rather as having an important underlying structure. Extraction of this *inner structure* has both experimental and theoretical significance. Knowledge of it, in principle, diminishes the *parametrization* needed to specify a flow.

A second important consequence of the new perspective is the idea that solutions of a dissipative system, of which the Navier-Stokes is an example, are attracted to low-dimensional manifolds. An estimate of the dimension of such an attractor furnishes an ideal value for the phase space needed to describe the system in question. Landau [20, 21] in an early investigation estimated the number of *degrees of freedom* that appear in a turbulent flow. Arguing that the smallest relevant length in a problem is the Kolmogorov scale η (the scale on which the flow becomes near Stokesian), the number of scales appearing in a length L is L/η . A straightforward calculation then shows that the number of degrees of freedom is given by [21]

$$(L/\eta)^3 = O(\text{Re}^{9/4}). \quad (1.1)$$

The same result, but as an estimate of the number of dimensions, has been confirmed in a mathematical treatment by Constantin et al. [22]. This result

is possibly misleading. Although special situations may be contrived in which the estimate (1.1) is actually necessary [23], it seems likely that the actual number of dimensions needed to characterize a non-pathological flow will be far less than this estimate.

To illustrate this point suppose we consider Rayleigh-Bénard (RB) convection (see section 2) in an infinite domain. Normally, for purposes of calculation the horizontal dependence is taken to be periodic, so that a spectral method can be applied [24]. In so doing, the flow at points one wavelength apart become completely correlated – which on physical grounds is clearly wrong. If a horizontal distance is doubled the unphysical correlation is deferred to distances of the order of twice the wavelength but the number of required *dimensions* is also doubled. In fact it is clear that the dimension estimate is *extensive!* From a practical point of view long-range correlations, since they are small, are not important and a calculation is physically sound as long as the scale of the computation is large compared with the correlation length. Moreover, the latter scale diminishes as the control parameter (the Rayleigh number in this instance) increases. We can suppose that the correlation length, roughly the largest eddy dimension, scales with distance from the boundary and the boundary layer thickness. (Kim [25] for the channel problem and Castaing et al. [26] for the RB problem have found indications that there is cross-talk between the top and bottom boundaries. If the gossip is significant some of the above remarks need to be reexamined.)

Another feature which needs scrutiny is the question of correlations across scale sizes. Landau's estimate (1.1) relates to the degrees of freedom and not to the fractal dimension of the attractor. If there is significant correlation among the degrees of freedom, then the number of relevant dimensions is accordingly diminished. There is some evidence for this being true as we show in section 4.

In the following sections we will discuss a variety of fluid and model flows which are chaotic and

for which large-scale computer simulations have been performed. With varying degrees of completeness we will discuss the dimension of the chaotic attractor in question. This discussion will be based in part on the calculation of the Lyapunov spectrum [27] and the associated attractor dimension estimate based on the Kaplan-Yorke formula [28], known as the Lyapunov dimension and denoted by d_L . The estimate of d_L furnishes us with the *size* of an ideal description. In section 3 we outline the Karhunen-Loeve [29, 30] method especially in the context of the present set of circumstances. This was introduced into the turbulence literature by Lumley [31, 32], who proposed it as a rational and objective procedure for the determination of coherent structures (see section 6). This method, furnishes us with a *near ideal* description.

2. Two problems

To explore the ideas raised in the Introduction we discuss computer simulations for two problems, each having two sub-problems. Complexity and machine limitations prevent the thorough examination of a true laboratory situation. Thus we will attempt to piece together a consistent picture drawn from problems created to furnish the pieces of the jigsaw.

2.1. Ginzburg-Landau equation [33]

The complex Ginzburg-Landau (GL) equation

$$\begin{aligned} G(A) = & A_t - q^2(i + c_0)A_{xx} \\ & - \rho A - (i - \rho)A|A^2| = 0 \end{aligned} \quad (2.1)$$

can be regarded as governing the perturbation amplitude in a variety of situations near critical stability [34–36]. The normalization of (2.1) has been given in earlier papers [37, 38]. Each of the three constants q^2, c_0, ρ are real and positive and

Newell's criterion [39]

$$0 \leq c_0 \leq 1/\rho \quad (2.2)$$

for instability will be assumed. In the simulations c_0 and ρ are taken to be constant ($c_0 = \rho = 0.25$) and q^2 is regarded as the active bifurcation parameter. It can be related to the square of the wavenumber and as it appears in (2.1), q^2 is a reciprocal Reynolds number.

The first of the two sub-problems, referred to as the slippery case, is specified by the boundary conditions

$$\frac{\partial A}{\partial x}(0) = \frac{\partial A}{\partial x}(\pi) = 0, \quad (2.3)$$

and the second problem, referred to as the sticky case, is specified by

$$A(0) = A(\pi) = 0. \quad (2.4)$$

This terminology is based on the analogy with the Rayleigh-Bénard (RB) convection problem (discussed later in the section). For the case of

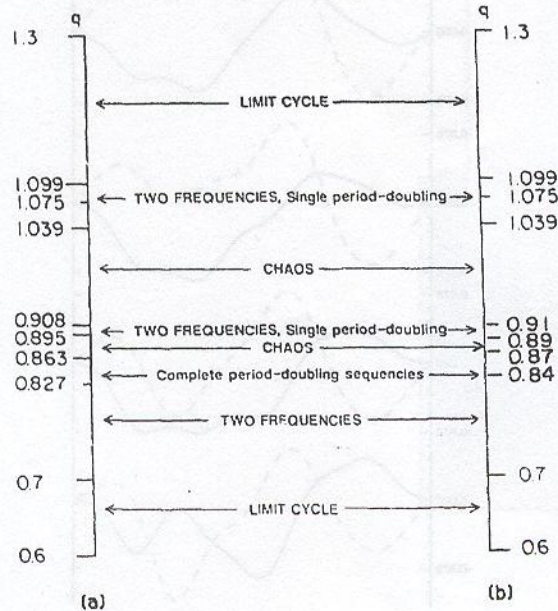


Fig. 1. (a) Summary of transitions for Ginzburg-Landau slippery boundary value problem. (b) Transitions for the three-mode approximation.

stressless boundary conditions in RB convection, the velocity parallel to a boundary has a zero normal derivative, but the velocity itself need not be zero so that the fluid can slip. At a material boundary in RB convection the fluid sticks to the wall and the velocity vanishes, (2.4).

It is easily seen that the GL equation respects odd and even symmetry with respect to x . Thus

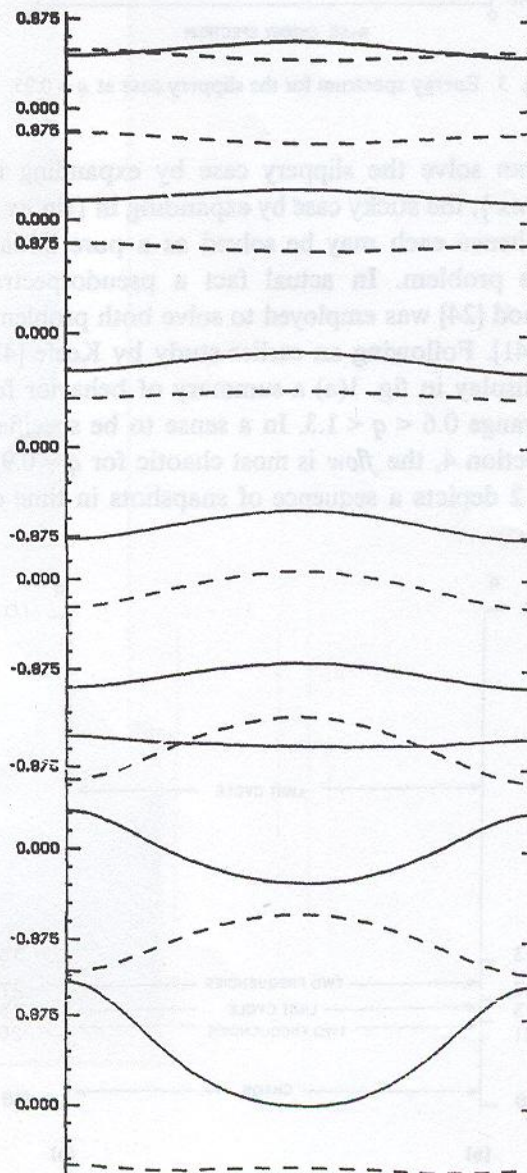


Fig. 2. Sequence of snapshots of A for the slippery case at $q = 0.95$. $\text{Re } A$ given by the continuous curve and $\text{Im } A$ by the dashed curve.

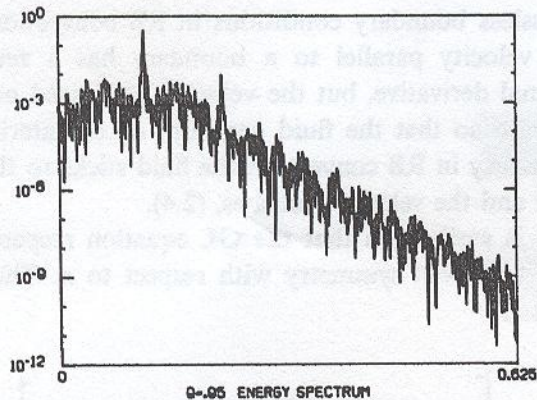


Fig. 3. Energy spectrum for the slippery case at $q = 0.95$.

we can solve the slippery case by expanding in $\{\cos nx\}$, the sticky case by expanding in $\{\sin nx\}$, and hence each may be solved as a pure initial-value problem. In actual fact a pseudospectral method [24] was employed to solve both problems [40, 41]. Following an earlier study by Keefe [42] we display in fig. 1(a) a summary of behavior for the range $0.6 < q < 1.3$. In a sense to be specified in section 4, the flow is most chaotic for $q = 0.95$. Fig. 2 depicts a sequence of snapshots in time of

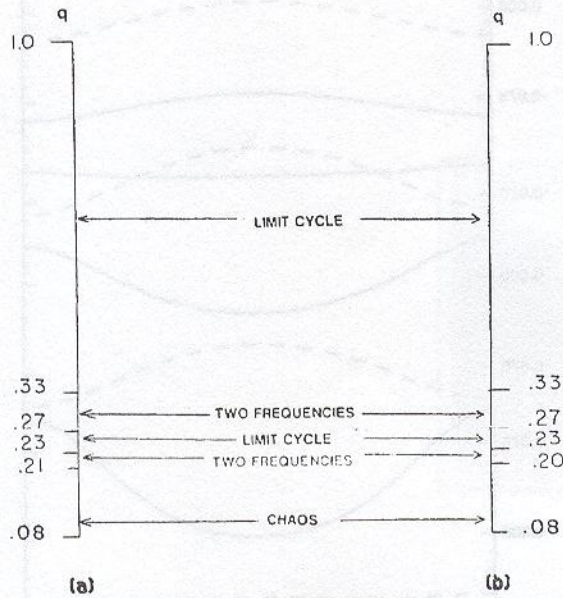


Fig. 4. (a) Summary of transitions for the Ginzburg-Landau sticky boundary value problem. (b) Transitions for the ten-mode approximations.

the complex amplitude, A , at this value of the Reynolds' number. The flow is seen to be smooth in space. On the other hand the temporal energy spectrum shown in fig. 3 implies that the flow is indeed chaotic.

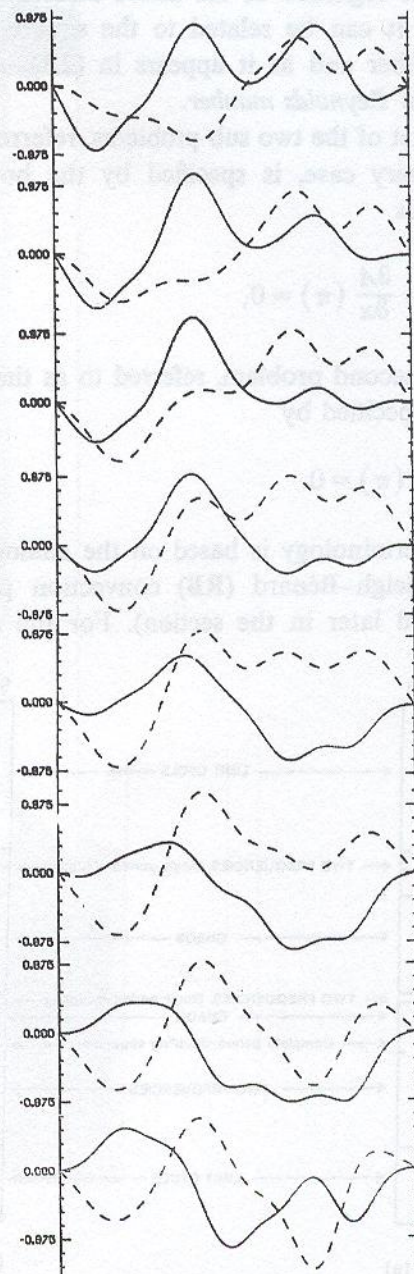


Fig. 5. Sequence of snapshots for the sticky case at $q = 0.14$. $\text{Re } A$ given by the continuous curve and $\text{Im } A$ by the dashed curve.

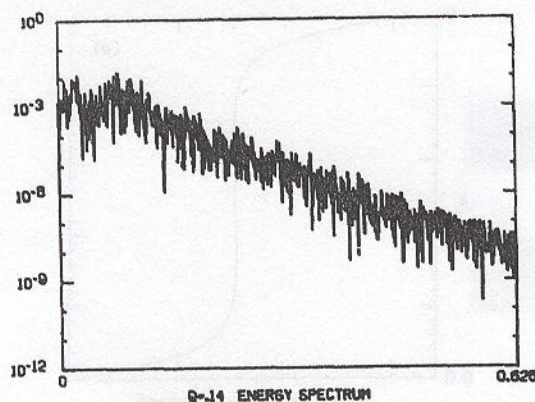


Fig. 6. Energy spectrum for the sticky case at $q = 0.14$.

A summary of results for the sticky boundary value problem is shown in fig. 4(a). By contrast with the slippery case, fig. 1(a), once chaos sets in, the flow does not relaminarize at a higher Reynolds' number. Fig. 5 depicts a sequence of snapshots of this flow at the reference Reynolds number $q = 0.14$. It appears that the flow has an element of spatial chaos as well as temporal chaos (shown in fig. 6).

Since the question of dimension is a recurring theme of this presentation, we mention that sixteen harmonics were found to adequately describe the slippery case over the range shown in fig. 1(a). Since the amplitude is complex this amounts to a phase space of 32 dimensions for the description of this case. By contrast the sticky case required 128 harmonics and thus a phase space of 256 dimensions for an adequate simulation.

2.2. Rayleigh-Bénard convection

2.2.1. Unbounded convection

RB convection has been extensively investigated [43–45] and as is well known is governed by the Boussinesq equations [46]

$$\begin{aligned} \nabla \cdot u &= 0, \\ \frac{du}{dt} + \nabla p &= \text{Ra Pr } e_z T + \text{Pr } \nabla^2 u, \\ \frac{dT}{dt} &= w + \nabla^2 T. \end{aligned} \quad (2.5)$$

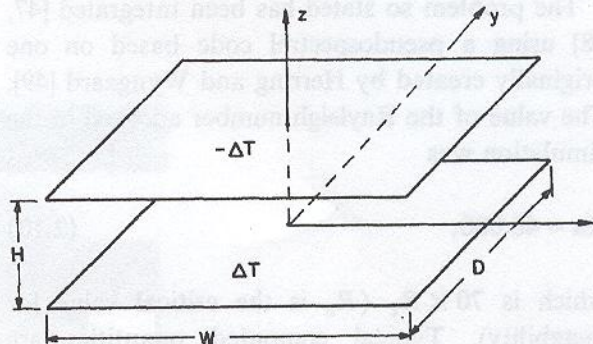


Fig. 7. Geometry for the Rayleigh-Bénard convection problems. In both cases the width, W , and depth, D , are taken equal.

There are two dimensionless parameters in (2.5), the Rayleigh number

$$\text{Ra} = \frac{g \Delta T H^3}{\kappa \nu} \quad (2.6)$$

and the Prandtl number

$$\text{Pr} = \nu / \kappa. \quad (2.7)$$

T represents the temperature measured from the linear conduction profile. This normalization and notation are standard [46] and discussion of these is not deemed necessary. A sketch of the geometry is given in fig. 7.

Two direct simulations of RB convection will be discussed in this paper. In the first case the flow is regarded as unbounded in the horizontal directions but L -periodic in both the x and y directions. (As discussed later imposing this symmetry leads to considerable data extension.) The vertical boundary conditions are

$$T = u \cdot n = \frac{\partial}{\partial n} u \wedge n = 0 \quad \text{at} \quad z = \pm H/2. \quad (2.8)$$

Here n denotes the normal at the bounding planes $z = \pm H/2$. Conditions (2.8) are the usual *stressless* or *slippery* boundary conditions [46]. The aspect ratio, H/L , is taken as

$$H/L = 2\sqrt{2} \quad (2.9)$$

so that the *most dangerous mode* is included [46].

The problem so stated has been integrated [47, 48] using a pseudospectral code based on one originally created by Herring and Wyngaard [49]. The value of the Rayleigh number adopted in the simulation was

$$Ra \approx 46,000, \quad (2.10)$$

which is $70 \times R_c$ (R_c is the critical value for instability). Typical computed quantities are shown in fig. 8. Additional measures of the flow are the Nusselt number, Nu, which indicates the efficiency of heat transport, and the Reynolds number based on the Taylor microscale, Re_T . The Nusselt number is given

$$Nu = \left(\frac{d\bar{T}}{dz} \right)_0 / (2\Delta T/H) = H/2\delta, \quad (2.11)$$

where $\bar{T}(z)$ denotes mean (ensembled averaged) total temperature (as shown in fig. 8) and the zero subscript indicates evaluation at a boundary. Eq. (2.11) defines an equivalent boundary layer thickness, δ . Another length scale, the Taylor microscale is implicit in the definition

$$Re_T = \frac{\langle w^2 \rangle}{\nu} \left\langle \left(\frac{\partial w}{\partial z} \right)^2 \right\rangle^{-1/2}, \quad (2.12)$$

(brackets denote ensemble averages). For the simulation discussed here we have

$$Nu \approx 6 \quad \text{and} \quad Re_T \approx 16. \quad (2.13)$$

In the actual simulation a lattice of $(32)^3$ points was employed. From (2.11) and (2.13) we see that the boundary layer is roughly $1/12$ the height and hence contains 2–3 grid points. It should also be noted that with three dependent variables (the three velocities are dependent because of continuity) and $(32)^3$ grid points the dynamics therefore takes place in a phase space of $O(10^5)$. Further details of the calculation can be found in refs. [47–49].

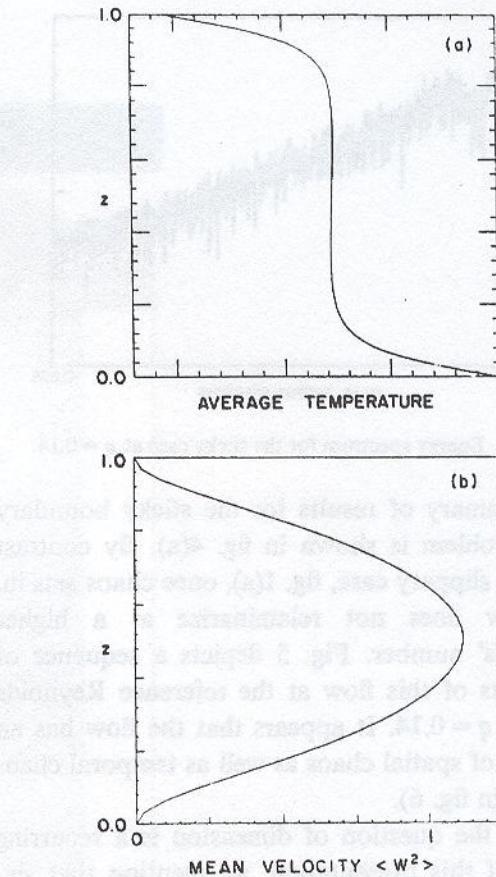


Fig. 8. (a) The average temperature $\langle T \rangle$ for the unbounded computation ($Ra \approx 46,000$). (b) The mean square velocity in vertical direction, $\langle w^2 \rangle$.

2.2.2. Bounded convection

In another simulation of RB convection we consider a bounded domain [50, 51]. For this simulation the boundary conditions (2.8) are augmented by

$$\begin{aligned} \mathbf{u} \cdot \mathbf{n} &= \frac{\partial}{\partial n} \mathbf{u} \wedge \mathbf{n} = \mathbf{n} \cdot \nabla T = 0 \\ \text{at } x &= \pm W/2, \quad y = \pm D/2, \end{aligned} \quad (2.14)$$

so that the periodicity requirement in the horizontal directions is dropped. For purposes of extending the data through group theory it is advantageous to take

$$W = D = L. \quad (2.15)$$

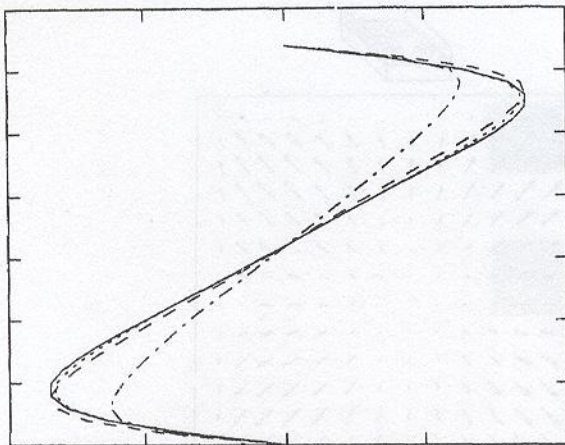


Fig. 9. The average temperature, from the bounded computation, taken at four locations on the diagonal from a corner to the center. Dot-dash signifies the corner location, long dash the next location, then the short dash, and finally the continuous curve gives the average temperature at the center.

The present case also may be posed as a pure initial-value problem. From this fact it can be shown that the critical Rayleigh number is the same as in the unbounded case [50]. In fact the stability analysis (of the conduction solution) can be found in Rayleigh's original analysis [52]. The resulting stability analysis shows that the most dangerous mode will be included if

$$H = L/2. \quad (2.16)$$

Unlike the unbounded case, bounded convection is not homogeneous in the xy plane. For example the profiles shown in fig. 8 do not depend on x and y , whereas the ensemble-averaged temperature now has such a dependence, see fig. 9. In fact the mean velocity $\langle u \rangle$ is now not equal to zero. Fig. 10 indicates the flow pattern for $\langle u \rangle$.

The calculations which we are discussing were carried out at the same value of Ra as the unbounded case, (2.10), namely $70 \times R_c$. For the same reasons discussed in the previous paragraph the Nusselt number depends on position and a contour plot of Nu is shown in fig. 11. From this we see that the variations are relatively small. It is also convenient to introduce the additional average

over the square $x-y$ planform

$$\bar{T} = \langle T \rangle_A = \frac{1}{WD} \int dx dy \langle T \rangle. \quad (2.17)$$

Plots of $\langle T \rangle_A$ and $\langle w^2 \rangle_A$ would be similar to those in fig. 8. The averaged value of the Nusselt number is

$$\langle Nu \rangle_A = 6.4 \quad (2.18)$$

which is comparable with (2.13).

In this instance the computational grid was taken as (16)³ which in view of (2.18) places between one and two grid points in the boundary layer. While this is somewhat coarse we deemed it adequate and trial calculations for a (32)³ grid confirmed our results. Thus the dynamics in this case takes place in a phase space of roughly $O(10^4)$ dimensions.

Further description of both flows as well as their analysis is left for later sections.

3. Karhunen–Loeve procedure

The K.L. procedure is textbook material [32] and we pause to give only a brief summary of the method specifically slanted towards the present context. Later, in section 6, we will comment on the relevance of the results of this procedure to the determination of coherent structures.

A chaotic or turbulent flow may be regarded as a point, moving in an infinite-dimensional space. The location of the point fully describes the flow at each instant of time. During the initial transient the point is drawn into an *attractor* for the system and moves in a chaotic fashion on this manifold. Ensemble averages of flow quantities can be regarded as time averages on the attractor. If ensemble averages are denoted by brackets then simple symmetry considerations for unbounded RB convection imply that

$$\langle u \rangle = 0. \quad (3.1)$$

(As already indicated this is not true for the case

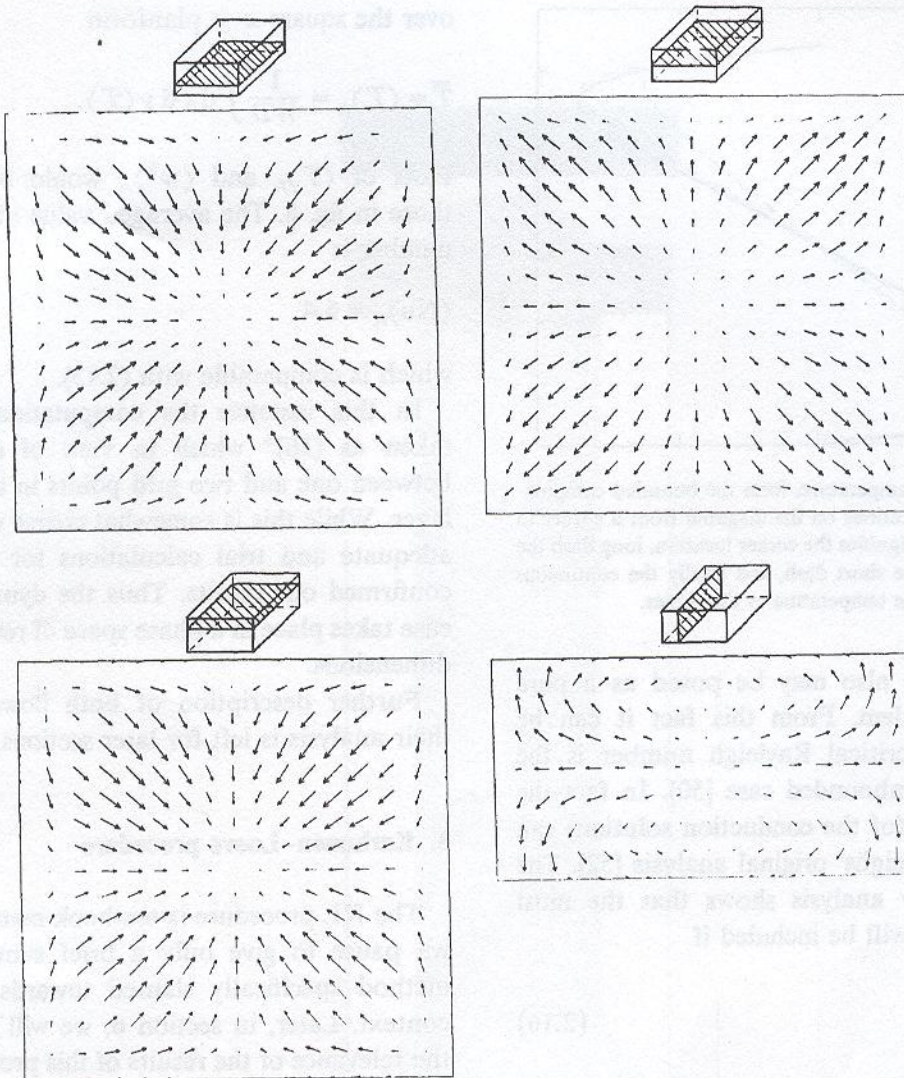


Fig. 10. The average velocity field $\langle u \rangle$ for the bounded case. The inserted sketches indicate the locations of the direction fields which are shown.

of bounded convection.) This is not true for the temperature and we write

$$T = \langle T \rangle + \theta \quad (3.2)$$

and henceforth consider

$$v = (u, \theta), \quad (3.3)$$

the flow fluctuation. (For the GL equation $\langle A \rangle = 0$.)

Next imagine an ensemble of states or snapshots of the flow, $\{v^{(n)}\}$, on the attractor,

$$v^{(n)} = v(x, t_n), \quad (3.4)$$

sampled at uncorrelated times t_n . To arrive at the KL procedure one can seek the most likely instantaneous flow, say given by $\phi(x)$, in the sense that

$$\lambda = \langle (v^{(n)}, \phi)^2 \rangle \quad (3.5)$$

is a maximum, subject to the normalization condition

$$(\phi, \phi) = \int \phi_k(x) \phi_k(x) dx = 1. \quad (3.6)$$

The solution to this problem is given by the principle eigenfunction of

$$\mathbf{K}\phi = \int \mathbf{K}(x, x') \phi(x') dx' = \lambda \phi(x), \quad (3.7)$$

where

$$\begin{aligned} K_{ij}(x, x') &= \langle v_i(x) v_j(x') \rangle \\ &= \frac{1}{N} \sum_{n=1}^N v_i^{(n)}(x) v_j^{(n)}(x') \end{aligned} \quad (3.8)$$

is the two-point correlation function (when not confusing, the superscript n will be dropped as in the brackets). \mathbf{K} is a non-negative hermitian operator and relation (3.7) generates a complete orthonormal set $\{\phi_n\}$ with eigenvalues $\lambda_n \geq 0$.

Finally (except for a set of zero measure) the flows can be expanded in the eigenfunctions $\{\phi_n\}$

$$v(x, t) = \sum_{n=1}^M a_n(t) \phi_n(x), \quad (3.9)$$

where convergence is in the L_2 sense. The coefficients a_n are statistically uncorrelated, i.e.

$$\langle a_n a_m \rangle = \lambda_n \delta_{nm}. \quad (3.10)$$

This is the essential content of the KL procedure [32]. These and related properties of this procedure strongly recommend its use in problems of chaotic or turbulent flows.

To assess the computation necessary to carry out the KL procedure consider the RB convection problem formulated in section 2. If we use a pseudo-spectral method with N points on a side this involves N^3 grid points. There are three dependent variables (the three velocities are related through continuity (2.5)). Thus a matrix approximation to \mathbf{K} will have $(3 \times N^3)^2$ entries. Even for

the most modest grid such an undertaking would exceed present computer resources. On the other hand for the one-dimensional GL calculations this direct method proves feasible. Also, in problems with two homogeneous directions such as unbounded RB convection problems, the eigenfunction dependence on the homogeneous directions are accounted for by sinusoids and the problem is reduced to an equivalent one-dimensional problem.

For the bounded RB problem there are no homogeneous directions. However one can resort to the method of snapshots [53]. This is based on the fact that (3.8) is a degenerate kernel and therefore an eigenfunction of \mathbf{K} can be represented as

$$\phi(x) = \sum_{n=1}^M \alpha_n v^{(n)}(x). \quad (3.11)$$

The problem of determining the α_n is then reduced to dealing with an $M \times M$ matrix. (This has been successfully used in an entirely different application [54, 55].)

It is worth noticing that the snapshot method is not seriously inhibited by high resolution (only the number of add-multiplies increases). Unlike the direct method, the complexity of the snapshot method only depends on M , the number of members of the ensemble. To illustrate this we consider an extension of the method, which will be given brief treatment since it will not be applied here. Imagine a phenomenon which is addition to being chaotic has a frequency spike (and harmonics) in its temporal spectrum. Lorenz [56] refers to this as noisy periodicity. The flow can now be conditionally sampled on the basis of the phase of the background periodicity. Thus each phase leads to its own ensemble of snapshots and as a result its own complete set of eigenfunctions. Next if this procedure is carried out for a sufficient set of phases we obtain a time-dependent set of eigenfunctions and from it a natural (KL) coordinate system that rotates in time.

Table I

i	λ_i
1	0.8599
2	0.1380
3	0.2108×10^{-2}

4. Eigenfunction analysis

4.1. Ginzburg-Landau equation

For both of the CL problems outlined in section 2 we form the correlation

$$K(x, x') = \langle A(x) A^*(x') \rangle \quad (4.1)$$

and solve the eigenfunction problem (3.7). For the slippery problem this is done for the bifurcation parameter $q = 0.95$ at which the Lyapunov dimension, d_L , is a maximum over the range, considered by us [40, 42] ($0.6 \leq q < 1.3$). On the other hand, for the sticky problem d_L appears to increase monotonically as q decreases and the correlation (4.1) is evaluated at the nominal value of $q = 0.14$.

Slippery. The first three eigenvalues are given in table I.

Since the mean energy of the motion is easily seen to be

$$\int_0^\pi \langle |A|^2 \rangle dx = \text{Tr } K = \sum_{n=1} \lambda_n \quad (4.2)$$

it follows that on average 99% of the total energy is captured by following just the first three modes. Examples of the eigenfunctions are shown in fig. 12. They are relatively poor in Fourier harmonics, a fact which is already signaled by the smooth looking snapshots of the flow shown in fig. 2.

Sticky. The first ten eigenvalues are shown in table II.

Unlike the case displayed in table I the fall off in energy is now much slower. Representative

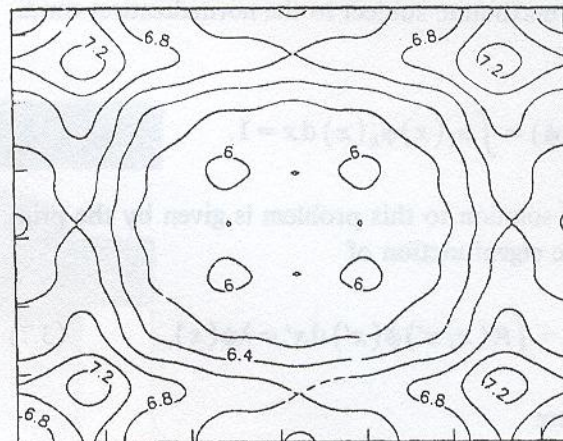


Fig. 11. Curves of constant heat flow at say the lower wall. The values shown give the local Nusselt number values.

Table II

i	λ_i	i	λ_i
1	0.2602	6	0.4987×10^{-1}
2	0.1997	7	0.2903×10^{-1}
3	0.1870	8	0.1349×10^{-2}
4	0.1334	9	0.7469×10^{-2}
5	0.1110	10	0.3810×10^{-2}

eigenfunctions are shown in fig. 13. These eigenfunctions are much richer in harmonics than in the slippery case, fig. 12, and as already indicated in fig. 5 the phenomenon itself seems to suggest spatial chaos.

4.2. Rayleigh-Bénard convection

For both convection simulations discussed in section 2 a high degree of symmetry was deliberately imposed on the geometry in order to affect a maximal extension of the database. Briefly stated, each symmetry element allows an additional flow field to be added to the pool of snapshots without an additional computation. As a consequence, however, this results in degenerate eigenspace since the correlation kernel, (3.8), must inherit the symmetry group of the flow geometry. This will be seen in each of the two cases which we now discuss.

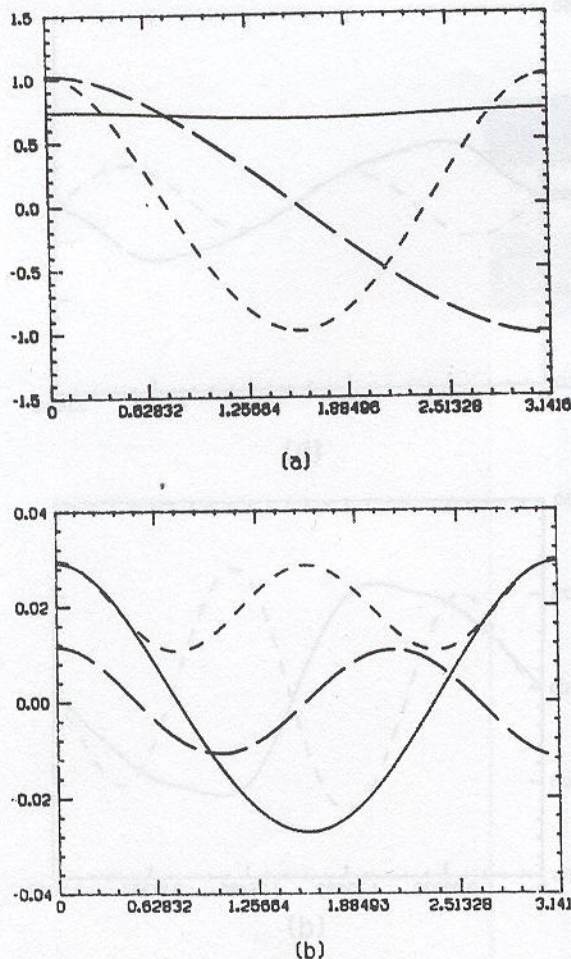


Fig. 12. First three Ginzburg-Landau eigenfunctions for the slippery case at $q = 0.95$. Continuous line refers to first, long dash to second and short dash to third eigenfunction. The real part is given in (a) and the imaginary part in (b).

4.2.1. Unbounded RB convection

In addition to the discrete symmetry group, which is composed of sixteen elements, the flow geometry is invariant under translations in the x and y directions [57]. As a consequence of this, the kernel \mathcal{K} has the form

$$\mathcal{K} = \mathcal{K}(x - x', y - y', z, z') \quad (4.3)$$

and from this it follows that the eigenfunctions must have the form

$$\phi = \phi(z; k, l) \exp(i2\pi(kx + ly)/L), \quad (4.4)$$

Table III
Principal eigenvalue for RB convection (unbounded)

k	l	q	λ_{kl}^q	Degeneracy	% of energy
0	1	1	0.303	4	41
1	1	1	0.065	4	9
0	1	2	0.031	4	4
0	0	1	0.025	2	1.7
0	2	1	0.021	4	2.8
1	2	1	0.014	8	3.8

where k and l are integers. Thus the eigenfunction problem becomes one-dimensional and may be expressed as

$$\int_0^H \mathcal{K}(k, l; z, z') \Phi_{kl}^q(z') dz' = \lambda_{kl}^q \Phi_{kl}^q(z), \quad (4.5)$$

where the kernel in (4.5) is the finite Fourier transform of (4.3). We will refer to k and l as wave-numbers and to q as the (vertical) quantum number.

In table III we list the first six eigenvalues. As was the case earlier, (4.2), the sum of the eigenvalues represents the mean energy and the last column gives the percent energy, on average, in the corresponding mode. Thus more than 60% of the energy is accounted for by the invariant subspaces of these six eigenvalues. The degeneracy of an eigenvalue is shown in the fifth column, and for example

$$\lambda_{01}^{(1)} = \lambda_{10}^{(1)} = \lambda_{-10}^{(1)} = \lambda_{0-1}^{(1)}. \quad (4.6)$$

Fig. 14 depicts an eigenfunction corresponding to this eigenvalue. The motion is made up of two counter rotating cells parallel to the y -axis. Heated fluid is moved to the top and the cooled fluid to the bottom. A second eigenfunction in this invariant subspace is obtained by translation by a quarter wave-length in the x -direction. The remaining two eigenfunctions are obtained by rotation by $\pi/2$ about the z -axis of the first two eigenfunctions.

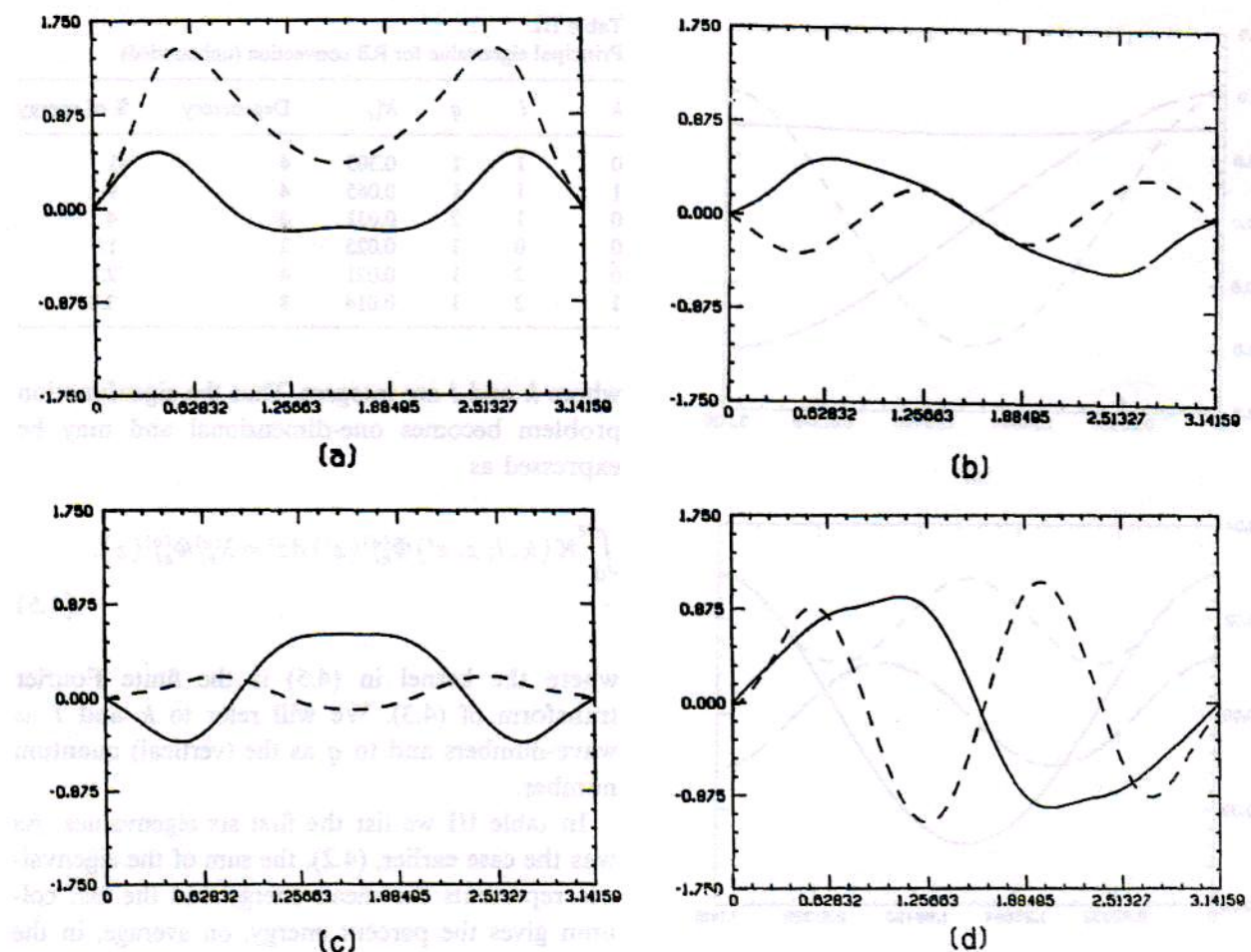


Fig. 13. First four Ginzburg-Landau eigenfunctions for the sticky case at $q = 0.14$ given in (a) through (d). The real part is given by the continuous curve and the imaginary part by the dashed curve.

4.2.2. Bounded RB convection

In this case only the discrete symmetry group applies, and the eigenfunctions no longer have the factorable property, (4.4), obtained previously. The (x, y, z) dependence of the eigenfunctions is intertwined and this property will bear on our discussion of coherent structures in section 6. Only a single index specifies an eigenvalue and a list of first six eigenvalues is shown in table IV.

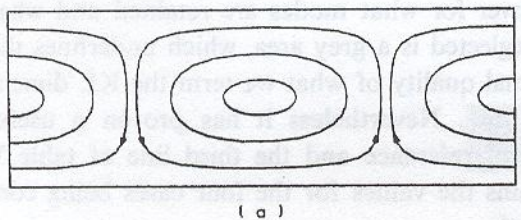
The eigenfunctions are now fully three-dimensional and their graphical representation is more difficult. An attempt at representing the principle eigenfunction is contained in fig. 15. This eigenfunction is a single roll convecting heated fluid to top and the cooled fluid to the bottom.

Table IV
Principle eigenfunction for RB convection (bounded)

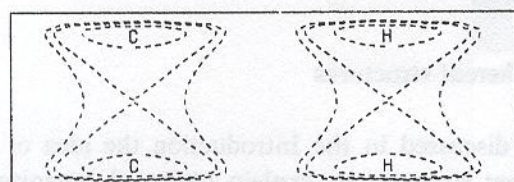
q	λ_q	Degeneracy	% of energy
1	0.2592	2	51.84
2	0.0337	2	6.74
3	0.0308	2	6.16
4	0.0030	1	0.3
5	0.0027	1	0.27
6	0.0024	1	0.24

The degeneracy is accounted for by rotating this structure through $\pi/2$ about the vertical.

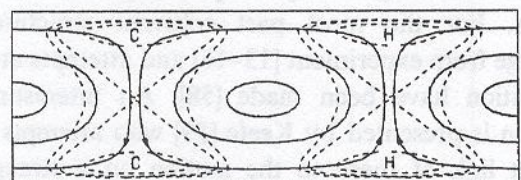
For each of the cases analyzed in this section we find that the eigenfunctions are composed of many harmonics (in the inhomogeneous directions). This



(a)



(b)



(c)

Fig. 14. One of the four principal eigenfunctions for the unbounded Rayleigh-Bénard computation. Streamlines are indicated as continuous curves (a) and isotherms as dashed curves (b), with the combination shown in (c). A second eigenfunction is obtained by translating this eigenfunction by a quarter wave. The remaining two eigenfunctions in the invariant subspace are obtained by a rotation of $\pi/2$ of the first two about the z-axis.

can be regarded as an indication that many different scales are *talking to one another* - or that there is a correlation between scales of the problem. Such a binding together of scales results in a net reduction in the number of degrees of freedom. It implies that although the smallest scale is necessary to resolve a boundary layer, not all the multiples of this scale are necessary to resolve the problem.

5. Attractor dimension

Each of the problems discussed in section 2 is described by partial differential equations and thus the representation of the evolution of each of the corresponding systems takes place in a space of an

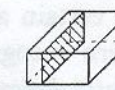
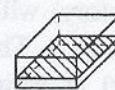
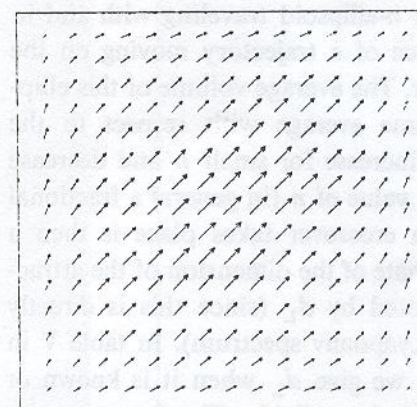
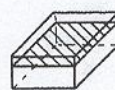
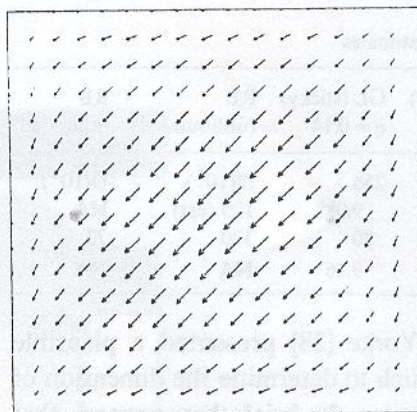


Fig. 15. Flow lines of the principle eigenfunction for the bounded Rayleigh-Bénard problem. The inserted sketches indicate the locations of the direction fields which are shown.

infinite number of dimensions. On a more practical note, since solution by numerical simulation was employed in each instance, the dimension of the representational space is really finite e.g. 32 for the GL slippery case and $O(10^5)$ for the unbounded RB convection. Furthermore since each of our systems is dissipative we expect that in each case there will be a chaotic attractor on which the solution trajectory travels and that this will be of relatively low dimension.

Table V
Various dimension estimates

	GL (slippery) $q = 0.95$	GL (sticky) $q = 0.14$	RB (unbounded)	RB (bounded)
d_N	32	256	$O(10^5)$	$O(10^4)$
d_L	3.047	9.088	125 (est)	NA
d_{KL}	6	20	320	70
\hat{d}_L	3.049	9.16	NA	NA

Kaplan and Yorke [28] presented a plausible procedure by which to determine the dimension of the chaotic attractor. In brief they propose that one consider an n -ellipsoid traveling with and in the tangent space of a trajectory moving on the chaotic attractor. The average volume of this ellipsoid (i.e. its time average with respect to the trajectory) will increase for small n and decrease for large n . The value of n (in general a fractional value) at which crossover takes place is then a reasonable estimate of the dimension of the attractor and is denoted by d_L (since this is directly related to the Lyapunov spectrum). In table V in the second row we give d_L when it is known or when an estimate is available. The first row contains the dimension of the space, d_N , in which the numerical simulation takes place.

In certain applications of the KL procedure in pattern recognition one finds the notion of the *intrinsic dimension* of the space as predicted by the KL procedure. These definitions are largely subjective and informal. In this same spirit we introduce d_{KL} and by it mean the number of actual eigenfunctions required so that the captured energy is at least 90% of the total (as measured by the energy norm) and that no neglected mode, on average, contains more than 1% of the energy contained in the principle eigenfunction mode. As stated these criteria are somewhat arbitrary and the second of these deserves a word or two. Since energy is essentially the square of an amplitude the second condition requires that we include into consideration all modes which have amplitudes one-tenth or more (on average) of that of the principal mode. In a manner of speaking this sets the *epsilon* of the problem to be one-tenth. The

crossover for what modes are retained and what are neglected is a grey area, which underlines the informal quality of what we term the KL dimension, d_{KL} . Nevertheless it has proven a useful point of reference and the third line of table V contains the values for the four cases being considered.

6. Coherent structures

As discussed in the Introduction the idea of a *coherent structure* to explain observed organized motions goes back more than thirty years, and in spite of this no generally accepted definition for it exists. For the most part coherent structures emerge from experiment [13–16] and attempts at a definition have been made [58]. An interesting notion is presented by Keefe [59] who attempts a direct link of these to the motion on a strange attractor.

The starting point for the present discussion is the work of Lumley [31, 32, 60], who was the first to suggest that the KL procedure be used to identify coherent structures. Although earlier work advocated the use of the KL procedure, especially in the context of weather forecasting [61], Lumley was the first to point out the power of the procedure (as summarized in section 3)* for identifying a coherent structure. We recall from section 3 that condition (3.5) requires that we find the maximally most probable instantaneous flow. It then follows that this is given by the principal eigenfunction of the two-point correlation function viewed as an operator. As a definition of a coherent structure this methodology is precise, objective and mathematically appealing.

There are however certain problems and perhaps conflicts with accepted observations of coherent structures. One problem arises when there are homogeneous directions in the flow. For exam-

*Lumley's development involves the correlation in time as well as space. For present purposes the additional generality is actually counter-productive and we do not factor it into our discussion, but see section 8.

ple for the unbounded RB convection both x and y are homogeneous and the kernel, \mathbf{K} , has the form (4.3). When this occurs the eigenfunctions become factorable, with a sinusoid accounting for the dependence in the homogeneous direction. For example (4.4) is sinusoidal in both the x and y directions. This is in clear conflict with experiment, since coherent structures are compact in space and sinusoids are in some sense the most non-compact functions.

It should be noted that a homogeneous direction in a numerical experiment in no way prevents the appearance of coherent structures. Perhaps the least controversial of coherent structures is the *hairpin vortex* first observed in the boundary layer by Theodorsen [8]. These same structures have been found in the computations of Moin and Kim [62] and of Krist and Zang [63]. In both instances the calculations are for channels with periodic streamwise and spanwise directions and hence homogeneous.

To account for the non-local behavior in a homogeneous direction Lumley [60] advanced the idea that the coherent structure be made of an admixture of principal eigenfunctions and that the composition of these be determined from a shot-noise [64] like procedure. Thus, in the context of unbounded RB convection, the suggestion is that the coherent structure, $\mathbf{U}(x, y, z)$, have the form

$$\mathbf{U}(x, y, z) = \sum_{k, l} \alpha_{kl} \Phi_{kl}^{(1)}(z) \exp(i2\pi(kx + ly)/L), \quad (6.1)$$

where the eigenfunctions $\Phi_{kl}^{(q)}$ are determined by (4.5). The constant coefficients α_{kl} are then such that

$$|\alpha_{kl}|^2 = \lambda_{kl}^{(1)}. \quad (6.2)$$

As motivation for the forms (6.1) and (6.2) we observe that the decomposition (3.9) in the present instance can be written as

$$\mathbf{v} = \sum_q V^{(q)}, \quad (6.3)$$

where

$$V^{(q)} = \sum_{kl} a_{kl}^{(q)} \Phi_{kl}^{(q)}(z) \exp(i2\pi(kx + ly)/L). \quad (6.4)$$

Then, since

$$\langle |a_{kl}^{(q)}|^2 \rangle = \lambda_{kl}^{(q)}, \quad (6.5)$$

we see that \mathbf{U} , (6.1), is to be associated with $V^{(1)}$. Only the magnitudes of α_{kl} in (6.1) are specified and a variety of procedures have been used for the determination of the phase of α_{kl} [65, 66]. In fact Moin and Moser present three different procedures for calculating the phases and report little difference in the forms obtained [65]. For the case of channel flow Moin and Moser find simple eddy structures composed of counter rotating rolls as a consequence of their construction.

In spite of the interesting structure just described, this form and those that might be associated with $V^{(q)}$, have meager theoretical basis and there is little reason to associate them with coherent structures. Moin and Moser [65] in fact refer to the construction (6.1) as a *characteristic eddy* and state that the relationship to a coherent structure is unclear. To set the stage for our later remarks we point out some of the shortcomings and weaknesses of the construction associated with (6.1).

As a starting point for this critique it should be noted that there is no a-priori reason to assemble a set of eigenfunctions on the basis of their quantum number q . In fact a detailed examination of the eigenfunctions shows that there is a certain amount of mode crossing for q held fixed and (k, l) varying. By modes we are referring to characterization of the eigenfunctions in terms of zero crossings (e.g. in Sturm-Liouville theory eigenfunctions and eigenvalues naturally assemble themselves in terms of the number of zero crossings [67], which is not true here). Thus, if it is the intention of this construction to assemble all first modes (for a vector eigenfunction this notion also needs some clarification), then q must be allowed

to vary. For the principal mode, the quantum number q for the most part will be unity by this criterion but for certain (k, l) , q will be two or even higher. If this detail is taken care of then the result of this construction will then be of the simple form of counter-rotating rolls, since this is dictated by restriction to the first mode. There is nevertheless nothing fundamental about the construction itself.

For some of the constructions it is reported that as much as 76% of the energy is captured by the $q = 1$ collection of eigenfunctions $\{\Phi_{kl}^1\}$. By this is meant that the energy ratio

$$r = \frac{\sum_{kl} \lambda_{kl}^{(1)}}{\sum_{k,l,q} \lambda_{kl}^{(q)}} \quad (6.6)$$

takes on a value as high as 0.76 (for the case of a wall sublayer of forty wall units [65]). However this can be somewhat misleading since the average energy in the direction U , (6.1), is given by

$$\frac{\langle |(\mathbf{u}, U)|^2 \rangle}{\langle U, U \rangle} = \frac{\sum_{kl} \lambda_{kl}^{(1)2}}{\sum_{kl} \lambda_{kl}^{(1)}} \quad (6.7)$$

The ratio of this to the total average energy in the subspace spanned by $\{\phi_{kl}^{(1)}\}$ is

$$\epsilon = \frac{\sum_{kl} \lambda_{kl}^{(1)2}}{(\sum_{kl} \lambda_{kl}^{(1)})^2} \quad (6.8)$$

which since $\lambda_{kl}^{(q)} \geq 0$ can be considerably less than unity. To further emphasize this point, we remark that (6.7) must be less than $\lambda_{01}^{(1)}$, a fact which follows from the optimization property of $\phi_{01}^{(1)}$ as discussed in section 3. Hence the reported energy actually residing in the characteristic eddy can be considerably less than the reported energy as given by (6.6). In fact, if the criterion for constructing an eddy is changed to capturing a certain amount of energy with the fewest eigenfunctions, then the chosen members should be included on the basis of the size of the associated eigenvalues.

The basis for the considerations leading to (6.1) is the appearance of homogeneous directions and the resultant non-compact eigenfunctions. For bounded RB convection there are no homogeneous directions and the issue of compactness never arises. As we saw in fig. 15 the principal eigenfunction is a roll motion, whereas it is generally accepted that *plumes* are the coherent structures [26] in turbulent convection (our database for both RB calculations has not yet been probed for plume structures).

It is suggested here that the above considerations, leading to (6.1), do not directly address the problem of isolating coherent structures. Perhaps the most widely accepted coherent structures are thermal plumes and hairpin vortices, both of which figured in the above discussion. Each of these is known to have a more or less defined time course beginning with a birth, ending with a disappearance and having an evolving structure in between. The eigenfunctions (and admixtures of them such as (6.1)) are time stationary and therefore cannot account for this process. Rather we suggest that particular eigenfunctions are players in the event known as a coherent structure. The collection of eigenfunctions which participates in this event do so to varying degrees as the sequence of steps defining a coherent structure unfolds. If this scenario is accepted then in order to identify a coherent structure we should examine the time courses of the coefficients $a_n(t)$, (3.9), for similar behavior. Alternatively the temporal energy spectrum of the players should show support in the same range. In this connection it should be noted that while the coefficients $\{a_n\}$ are uncorrelated, (3.10) over long times, this does not exclude important short-time interaction. This might also be investigated by looking into third-order correlations such as

$$c_{nm} = \langle |a_n|^2 a_m \rangle, \quad (6.9)$$

where a_n is a likely participant for the set involved in the coherent structure and a_m is a candidate. These ideas need to be explored further, and are conjectural at this point.

7. Reduced dynamics

The eigenfunction developments produced for each of the problems considered here can in a straightforward way be used to approximate the dynamic behavior of the corresponding system [68]. In each instance the Lyapunov dimension estimate furnishes us with the ideal goal for such an approximation. However, since this dimension estimate does not also furnish a basis set for the underlying attractor, we fall back on the KL procedure for an approximate basis set. Thus if a typical dynamical system is denoted by

$$\frac{\partial \mathbf{v}}{\partial t} = D(\mathbf{v}) \quad (7.1)$$

and the KL (orthonormal) eigenfunction are $\{\phi^{(n)}\}$ then the Galerkin approximation [69] first projects \mathbf{v}

$$\mathbf{v}_N = P_N \mathbf{v} = \sum_{n=1}^N (\phi^{(n)}, \mathbf{v}) \phi^{(n)} = \sum_{n=1}^N a_n \phi^{(n)} \quad (7.2)$$

and then projects (7.1)

$$\left(\phi^{(k)}, \frac{\partial}{\partial t} \mathbf{v}_N - D(\mathbf{v}_N) \right) = 0, \quad k = 1, N. \quad (7.3)$$

The result is a system of N dynamical equations

$$\frac{d\alpha}{dt} = F(\alpha) \quad (7.4)$$

in the reduced state vector,

$$\alpha = (a_1, \dots, a_N). \quad (7.5)$$

While the overall picture for achieving the reduced dynamics (7.4) is clear certain inferences and implications require mention.

A first consideration is the criterion for choosing a basis in the projected space. This is taken on the basis of energy, i.e. the eigenfunctions are ordered according to decreasing values of the

eigenvalues $\lambda_1 \geq \lambda_2 \geq \lambda_3 \dots$, and the truncation decided by the KL dimension d_{KL} as stated in section 5. As discussed in the previous section other criteria can be given.

Another consideration is the range of validity of the approximate system, (7.4). Specifically the eigenfunctions $\{\phi^{(n)}\}$ in each instance have been generated for fixed values of the control parameters. Is there a range of validity for the reduced dynamical system, in parameter space, beyond these fixed values?

7.1. GL problems

As indicated in table V, d_{KL} for the slippery case is 6 and for the sticky case is 20. In the first instance a system of 3 complex and in the second a system of 10 complex equations are derived from the Galerkin procedure, (7.3) [38, 41]. Figs. 1b and 4b summarize the behavior found for these reduced systems over the same range over which the exact results have been described in figs. 1a and 4a. The agreement is excellent not only in this respect but also in many fine details which we do not go into here [41]. Finally the last row of table V compares the Lyapunov dimension for the reduced dynamical system with the exact value given in the second row. The agreement is also very good and remains so throughout the the parameter range considered by us [41].

7.2. RB convection

Only fragmentary results are available in this instance. For the unbounded case the KL dimension, d_{KL} , is 320 and a system of 320 equations has been generated to describe the dynamics [70]. The resulting system produces results that are about 8% in error when compared with exact results. For example the Nusselt number is found to be $\text{Nu} = 6.5$ instead of $\text{Nu} = 6$, (2.13). Techniques based on an *eddy viscosity* are now being explored in order to improve on these results.

Finally before concluding this section we mention the very interesting investigation by Aubry

et al. [71]. They consider the channel flow problem and also consider the possibility of modeling the phenomena by a low-dimensional system. Since their goal was not quantitative agreement they drastically reduced the size of their system to a set of ten differential equations based largely on the first mode or characteristic eddy as described in section 6. (Keefe has estimated the Lyapunov dimension of this system, at a near transition Reynolds number, to be roughly $d_L \approx 400$.) As in the actual physical situation their system exhibits a bursting evolution in time. Encouraging as this is, it remains to be seen how much the system needs to be extended in order to go beyond just qualitative agreement with the physics.

8. Concluding remarks

The present paper represents the contents of the lecture given at the Los Alamos meeting. During the course of the lecture and in the discussions afterward interesting questions and points were raised. This often resulted in a sharpening of ideas and much of this has found its way into the text. Two such issues are addressed in this section since they did not naturally arise in the course of writing up the lecture.

The first issue concerns the ability of the methods advocated in this manuscript to deal with the rapid temporal effects found for example, in a boundary layer (see Landahl [72] in this volume). To illustrate this point we consider the temporal as well as spatial correlation function as defined by

$$R_{ij}(x, y, t, t') = \langle u_i(x, t) u_j(y, t') \rangle, \quad (8.1)$$

and which is sometimes referred to as the structure function. Lumley, in fact, in his original treatment [31] considers (8.1) and not (3.8). Since the Navier-Stokes equations are autonomous the correlation (8.1) is translationally invariant in time

$$R_{ij}(x, y, t, t') = R_{ij}(x, y, t - t'). \quad (8.2)$$

Thus $K_{ij}(x, y)$ is obtained by setting $t = t'$

$$K_{ij}(x, y) = R_{ij}(x, y, 0), \quad (8.3)$$

and therefore temporal effects are lost.

We first observe that the eigenfunctions of R_{ij} are sinusoidal in the time domain, which does not help in isolating a phenomenon such as bursting. By setting $t = t'$ and eliminating time we do not eliminate the phenomenon of bursting, a fact which is clearly indicated by the work of Aubry et al. [71]. The main criterion for capturing the sequence of events found in a burst is that the ensemble of snapshots be sufficiently rich in events. For example if the subevents occurring in a burst form part of the ensemble then they have been incorporated in the eigenfunctions. Experience has taught us that even a meager ensemble produces a rich set of eigenfunctions.

A second issue is the question of whether the neglect of low-energy modes can seriously alter the dynamics. Examples abound in classical dynamics where small energy changes produce dramatic changes in behavior. For example the simple pendulum depends sensitively on energy as to whether libration or rotation occurs. However this is a system with a high degree of symmetry, and all systems known to us which have this sensitive dependence on small bits of energy have this high degree of symmetry. For the systems we have been discussing there are many geometrical symmetries and one might wonder if the same thing can occur. But once the system has become chaotic the symmetries are lost, as is the sensitive dependence. Symmetries are preserved only in the statistical sense. To illustrate this point we might consider the RB convection problems. The orbit of the system has no knowledge of the sixteen symmetries of the system except in the overall statistics. Thus for example there is no degeneracy in the Lyapunov spectrum. We believe that this state of affairs is typical for turbulent flows and that one need not be concerned about the neglect mode carrying relatively small amounts of energy.

Acknowledgements

The work reported here was supported by DARPA-URI N00014-86-K0754.

References

- [1] E. Lorenz, *J. Atmos. Sci.* 20 (1967) 130.
- [2] D. Ruelle and F. Takens, *Commun. Math. Phys.* 20 (1971) 167.
- [3] M.J. Feigenbaum, *J. Stat. Phys.* 19 (1978) 25.
- [4] J. Guckenheimer and P. Holmes, *Nonlinear Oscillations, Dynamical Systems and Bifurcation of Vector Fields* (Springer, New York, 1983).
- [5] P. Bergé, Y. Pomeau and C. Vidal, *Order Within Chaos* (Wiley, New York, 1986).
- [6] G.S. Schuster, *Deterministic Chaos: An Introduction* (Physik-Verlag, Weinheim, FRG, 1984).
- [7] H.E. Helleman (ed.), *Nonlinear Dynamics*, (New York Academy of Science, 1980).
- [8] T. Theodorsen, Mechanism of turbulence, in: Proc. 2nd Midwestern Conf. on Fluid Mechanics, Ohio State Univ. Columbus, OH (1952).
- [9] Townsend, *The Structure of Turbulent Shear Flow* (Camb. Univ. Press, Cambridge, 1956).
- [10] S.J. Kline, W.C. Reynolds, F.A. Schraub and P.W. Runstadler, *J. Fluid Mech.* 30 (1967) 741.
- [11] G.L. Brown and A. Roshko, *J. Fluid Mech.* 64 (1974) 775.
- [12] R.E. Falco, *Phys. Fluids* 12 (1977) 426.
- [13] R.F. Blackwelder and R.E. Kaplan, *J. Fluid Mech.* 76 (1976) 89.
- [14] S.S. Lu and W.W. Willmarth, *J. Fluid Mech.* 60 (1973) 481.
- [15] A.K.M.F. Hussain, *Phys. Fluids* 26 (1983) 2816.
- [16] B.J. Cantwell, *Ann. Rev. Fluid Mech.* 13 (1983) 457.
- [17] Mallory, *Morte d'Arthur* (Scribner, New York, 1982).
- [18] G.I. Taylor, Statistical theory of turbulence, Pts. I-V, *Proc. R. Soc. London A* 151, p. 421.
- [19] T. von Karman and L. Howarth, On the statistical theory of isotropic turbulence, *Proc. R. Soc. London A* 164 (1938) 192–215.
- [20] L.D. Landau, *Dok. Akad. Nauk. SSSR* 44 (1944) 339–342.
- [21] L.D. Landau and E.M. Lifshitz, *Fluid Mechanics* (Pergamon, Oxford, 1986).
- [22] P. Constantin, C. Foias, O.P. Manley and R. Temam, *J. Fluid Mech.* 150 (1985).
- [23] A.V. Bobin and M.I. Visile, *Russ. Math. Survey* 38 (1983) 151–213.
- [24] C. Canuto, M.Y. Hussaini, A. Quarderonic and T.A. Zang, *Spectral Methods in Fluid Dynamics* (Springer, New York, 1987).
- [25] J. Kim, private communication.
- [26] B. Castaing, G. Gunaratne, F. Heslot, L. Kadanoff, A. Libschaber, S. Thomae, X.-Z. Wu, S. Zaleski and G. Zanetti, Scaling of hard thermal turbulence in Rayleigh-Bénard convection (submitted for publication).
- [27] J.D. Farmer, E. Ott and J.A. Yorke, *Physica* 7 (1983) 153.
- [28] J. Kaplan and J. Yorke, Functional differential equations and the approximation of fixed points, in: *Lecture Notes in Mathematics* 730 (Springer, Berlin, 1978) p. 228.
- [29] K. Karhunen, *Ann. Acad. Sci. Fenniae, Ser A1, Math. Phys.* 37 (1946).
- [30] M.M. Loeve, *Probability Theory* (van Nostrand, Princeton, NJ, 1955).
- [31] J.L. Lumley, The structure of inhomogeneous turbulent flows, in: *Atmospheric Turbulence and Radio Wave Propagation*, A.M. Yaglom and V.I. Tatarski, eds. (Nauka, Moscow, 1967) pp. 166–178.
- [32] J.L. Lumley, *Stochastic Tools in Turbulence* (Academic Press, New York, 1970).
- [33] V.L. Ginzburg and L.D. Landau, *Zh. Eksp. Teor. Fiz.* 20 (1950).
- [34] A.C. Newell and J.A. Whitehead, *J. Fluid Mech.* 38 (1969) 279.
- [35] S. Kogelman and R.D. DiPrima, *Phys. Fluids* 13 (1970) 1.
- [36] K. Stewartson and J.T. Stuart, *J. Fluid Mech.* 48 (1979) 529.
- [37] L. Sirovich and P.K. Newton, in: *Stability of Time Dependent and Spatially Varying Flows*, D.L. Dwoyer and M.Y. Hussaini, eds. (Springer, New York, 1986).
- [38] L. Sirovich and J.D. Rodriguez, *Phys. Lett. A* 120 (1987) 211.
- [39] A.C. Newell, in: *Nonlinear Wave Motion*, A.D. Newell, ed. (AMS, Providence, RI, 1974).
- [40] L. Sirovich, J.D. Rodriguez and B.W. Knight, Two Boundary Value Problems for the Ginzburg-Landau Problem (submitted for publication).
- [41] J.D. Rodriguez and L. Sirovich, Low Dimensional Dynamics for the complex Ginzburg-Landau Equation (submitted).
- [42] Keefe, *Stud. Appl. Math.* 73 (1985) 91.
- [43] F.H. Busse and R.M. Clever, *J. Fluid Mech.* 91 (1979) 319–335.
- [44] F.H. Busse and J.A. Whitehead, *J. Fluid Mech.* 47 (1971) 305–320.
- [45] F. Busse, *Proc. IUTAM Symp. Inst. Cont. Syst., Herrenberg*, (Springer, Berlin, 1971).
- [46] P.G. Drazin and W.H. Reid, *Hydrodynamic Stability* (Cambridge Univ. Press, Cambridge, 1981).
- [47] L. Sirovich, M. Maxey and H. Tarman, Analysis of turbulent thermal convection, 6th Symp. on Turbulent Shear Flow, Toulouse, France (1987).
- [48] L. Sirovich, H. Tarman and M. Maxey, An eigenfunction analysis of turbulent thermal convection, B.E. Launder, ed. (Springer, Berlin, 1988).
- [49] J.H. Herring and J. Wyngaard, Convection with a simple chemically reactive passive scalar, in: 5th Symp. on Turbulent Shear Flows, Cornell (1985) 10.39–10.43.
- [50] L. Sirovich and H. Park, Turbulent thermal convection in a finite domain: theory (to be submitted).
- [51] H. Park and L. Sirovich, Turbulent thermal convection in a finite domain: numerical experiments and results (to be submitted).

- [52] Lord Rayleigh, *Phil. Mag.* 32 (1916) 529–546.
- [53] L. Sirovich, *Q. Appl. Math.*, 45 (3) (1987) 561–571.
- [54] L. Sirovich and M. Kirby, *J. Opt. Soc. Am. A* 4 (3) (March 1987).
- [55] M. Kirby and L. Sirovich, The application of the Karhunen–Loeve Procedure for the characterization of human faces (submitted for publication).
- [56] E.N. Lorenz, Noisy periodicity and reverse bifurcation, in: *Nonlinear Dynamics*, R.H.G. Helleman, ed. (New York Academy of Science, 1980).
- [57] L. Sirovich, *Q. Appl. Math.*, 45 (3) (1987) 573–582.
- [58] A.K.M.F. Hussain, *J. Fluid Mech.* 173 (1986) 303.
- [59] L.R. Keefe, Connecting coherent structures and strange attractors (1988).
- [60] J.L. Lumley, Coherent structures in turbulence, in: *Transition and Turbulence*, R.E. Meyer, ed., (Academic, New York, 1981).
- [61] E.N. Lorenz, Prospects for statistical weather forecasting, Final Report, Statistical Forecasting Project, MIT (1954).
- [62] P. Moin and J. Kim, *J. Fluid Mech.* 155 (1985) 441.
- [63] S.E. Krist and T.A. Zang, NASA TP 2667 (1987).
- [64] S.O. Rice, *Bell Syst. Tech. J.* 23 (1944) 283.
- [65] P. Moin and R.D. Moser, *J. Fluid Mech.* (1988) (to appear).
- [66] S. Herzog, The large scale structure in the near-wall region of turbulent pipe flow, Thesis, Cornell University (1986).
- [67] G. Birkhoff and G.C. Rotta, *Ordinary Differential Equations* (Ginn, Boston, MA, 1962).
- [68] L. Sirovich, *Q. Appl. Math.*, 45 (3) (1987) 583–590.
- [69] L.V. Kantorovich and V.I. Krylov, *Approximate Methods of Higher Analysis* (Interscience, New York 1958).
- [70] H. Tarman and L. Sirovich, Reduced dynamics for the turbulent convection problem (to appear).
- [71] N. Aubry, P. Holmes, J.L. Lumley and E. Stone, *J. Fluid Mech.* 192 (1988) 115–175.
- [72] M. Landahl, these Proceedings, *Physica D* 37 (1989) 11.